Third International Symposium on the Effects of Surface Geology on Seismic Motion
Grenoble, France, 30 August - 1 September 2006
Paper Number: S12

Numerical Modeling of Earthquake Motion in Grenoble Basin, France, Using a 4th-order Velocity-stress Arbitrary Discontinuous Staggered-grid FD Scheme

Jozef KRISTEK[1,2], Peter MOCZO[1,2], Peter PAZAK[1]
1 Faculty of Math., Physics and Informatics, Comenius University, Bratislava, Slovakia
2 Geophysical Institute, Slovak Academy of Sciences, Bratislava, Slovakia

ABSTRACT - Numerical simulations of the earthquake motion in a deep Alpine Grenoble basin, France, were performed for the flat-free surface model of Grenoble basin and for four detailed kinematic source models (W1, W2, S1, S2) specified for participants of the ESG 2006 Grenoble basin benchmark. A 3D 4th-order velocity-stress finite-difference scheme (Moczo et al. 2002, Kristek et al. 2002, Kristek et al. 2003, Moczo et al. 2004) on an arbitrary discontinuous staggered grid was used for simulations.

1. Introduction

There are several numerical methods that can be applied in order to simulate earthquake ground motion in a deep sediment-filled valley such as the sedimentary basin beneath the city of Grenoble in French Alps. The methods include recent formulations of the finite-difference method (e.g., Takeuchi and Geller 2000, Moczo et al. 2002, Kristek and Moczo 2003, Kang and Baag 2004) and the finite-element method (e.g., Bielak et al. 2003, Yoshimura et al. 2003), as well as the spectral-element method (e.g., Komatitsch et al. 2004, Chaljub et al. 2006) and ADER-DG method (Käser and Dumbser 2006). The four mentioned methods differ in accuracy with respect to different structural features of the complex heterogeneous models and considerably in the computational efficiency.

The finite-difference method can be considered as the simplest method from the mathematical point of view. Recent development in application of the method to seismic wave propagation confirms, in our opinion, that the achievable level of accuracy and computational efficiency in the case of relatively complex structural models makes the method still an important numerical tool in seismological research, mainly in earthquake ground motion prediction and analysis.

We hope that our finite-difference simulations for the ESG 2006 Grenoble basin benchmark will prove that our finite-difference scheme can be well applied to as structurally complex models as the Grenoble valley is.

2. Method of Simulation: 3D 4th-order Velocity-stress Finite-difference Staggered-grid Scheme for a Heterogeneous Viscoelastic Medium

For numerical simulations we used a 3D 4th-order velocity-stress finite-difference staggered-grid scheme for a heterogeneous viscoelastic medium. A complete theory and presentation of the scheme can be found in papers by Moczo et al. (2002), Kristek et al. (2002), Kristek et al. (2003), Moczo et al. (2004) and Moczo and Kristek (2005).

The finite-difference scheme solves the equation of motion and Hooke's law for viscoelastic medium with rheology of the generalized Maxwell body in the following formulation:

$$\rho \dot{v}_i = \sigma_{ij},_j + f_i \tag{1}$$

and

$$\begin{aligned} \dot{\sigma}_{ij} &= \kappa \dot{\varepsilon}_{kk} \delta_{ij} + 2\mu\left(\dot{\varepsilon}_{ij} - \tfrac{1}{3}\dot{\varepsilon}_{kk}\delta_{ij} \right) \\ &\quad - \sum_{l}^{4} \left[\kappa Y_l^{\kappa} \xi_l^{kk} \delta_{ij} + 2\mu Y_l^{\mu} \left(\xi_l^{ij} - \tfrac{1}{3}\xi_l^{kk}\delta_{ij} \right) \right], \end{aligned} \tag{2}$$

$$\dot{\xi}_l^{ij} + \omega_l \xi_l^{ij} = \omega_l \dot{\varepsilon}_{ij} \quad ; \quad l = 1,\dots,4 \; . \tag{3}$$

Here, in a Cartesian coordinate system (x_1, x_2, x_3), $\rho(x_i)$; $i \in \{1,2,3\}$ is density, $\kappa(x_i)$ unrelaxed (elastic) bulk modulus, $\mu(x_i)$ unrelaxed shear modulus, Y_l^{κ} and Y_l^{μ} anelastic coefficients, $\vec{u}(x_i, t)$ displacement vector, t time, $\vec{f}(x_i, t)$ body force per unit volume, $\sigma_{ij}(x_k, t)$ and $\varepsilon_{ij}(x_k, t)$; $i, j, k \in \{1,2,3\}$ stress and strain tensors, ξ_l^{ij} material-independent anelastic functions (material-independent memory variables), and ω_l relaxation angular frequencies. The anelastic coefficients Y_l^{κ} and Y_l^{μ} are obtained from

$$Y_l^{\kappa} = \left(\alpha^2 Y_l^{\alpha} - \tfrac{4}{3}\beta^2 Y_l^{\beta} \right) \Big/ \left(\alpha^2 - \tfrac{4}{3}\beta^2 \right) \quad , \quad Y_l^{\mu} = Y_l^{\beta} \quad ; \; l = 1,\dots,4 \; , \tag{4}$$

where $\alpha = \left[\left(\kappa + \tfrac{4}{3}\mu \right) / \rho \right]^{1/2}$ and $\beta = (\mu/\rho)^{1/2}$ are elastic (that is, corresponding to the unrelaxed moduli) P and S wave velocities, and anelastic coefficients Y_l^{α} and Y_l^{β} are obtained from the desired or measured quality factor values Q_{α} and Q_{β} using the system of equations

$$Q_{\nu}^{-1}\left(\tilde{\omega}_k\right) = \sum_{l=1}^{n} \frac{\omega_l \tilde{\omega}_k + \omega_l^2 Q_{\nu}^{-1}\left(\tilde{\omega}_k\right)}{\omega_l^2 + \tilde{\omega}_k^{\,2}} Y_l^{\nu} \quad ; k = 1,\dots,7 \, , \quad \nu \in \{\alpha, \beta\}. \tag{5}$$

We cannot go into details of the finite-difference schemes for solving equations (1) to (3). All details can be found in the references given above. Here we only comment that the schemes for solving the equation of motion and time derivative of Hooke's law have the same structure as standard 4th-order velocity staggered-grid schemes. The accuracy of our scheme is due to the way how we treat smooth material heterogeneity and material discontinuity. For brevity we give here only formulas for evaluation of effective grid density and unrelaxed moduli assigned to respective grid positions:

$$\rho_{I,\,J+1/2,\,K+1/2}^{A} = \frac{1}{h^3} \int_{x_{I-\frac{1}{2}}}^{x_{I+\frac{1}{2}}} \int_{y_J}^{y_{J+1}} \int_{z_K}^{z_{K+1}} \rho \,\mathrm{d}x\,\mathrm{d}y\,\mathrm{d}z \; , \tag{6}$$

$$\kappa^{H}_{I+1/2,\ J+1/2,\ K+1/2} = \left[\frac{1}{h^3} \int\limits_{x_I}^{x_{I+1}} \int\limits_{y_J}^{y_{J+1}} \int\limits_{z_K}^{z_{K+1}} \frac{1}{\kappa}\, \mathrm{d}x\ \mathrm{d}y\ \mathrm{d}z \right]^{-1} \tag{7}$$

and

$$\mu^{H}_{I+1/2,\ J+1/2,\ K+1/2} = \left[\frac{1}{h^3} \int\limits_{x_I}^{x_{I+1}} \int\limits_{y_J}^{y_{J+1}} \int\limits_{z_K}^{z_{K+1}} \frac{1}{\mu}\, \mathrm{d}x\ \mathrm{d}y\ \mathrm{d}z \right]^{-1} . \tag{8}$$

It is clear from eq. (6) that an effective grid density for a corresponding particle velocity component is evaluated as an integral volume arithmetic average of density inside a $h \times h \times h$ grid cell centered at the grid position of the corresponding particle velocity component. The integral is evaluated numerically and the grid cell can contain a material discontinuity. Effective grid unrelaxed bulk and shear moduli are evaluated as integral volume harmonic averages of moduli in respective grid cells centered at grid positions of the stress-tensor components, eqs. (7) and (8).

Anelastic coefficients Y_l^{κ} and Y_l^{μ} for a grid cell containing smoothly heterogeneous medium and/or material interface are determined as follows: An average viscoelastic modulus in the frequency domain is numerically determined for a cell as an integral harmonic average. A corresponding quality factor is then determined from the averaged viscoelastic modulus at specified frequencies. Equations (5) for the bulk and shear moduli are then used to determine average anelastic functions.

Spatial distribution of the material parameters and field functions is shown in Fig. 1.

3. Arbitrary Discontinuous Staggered Grid

In numerical simulations for surface heterogeneous structures it often is possible have coarser spatial sampling in the lower part of the computational region: a near-surface sedimentary body with lower seismic wave velocities (covered by a finer spatial grid) is underlain by a stiffer bedrock with larger seismic wave velocities (covered by a coarser spatial grid). The use of such a combined spatial grid is extremely important because it significantly reduces computer memory requirement and computational time.

In order to make such a combined (or discontinuous) spatial grid efficient, the ratio of the size of a spatial grid spacing in the coarser grid and that in the finer grid should

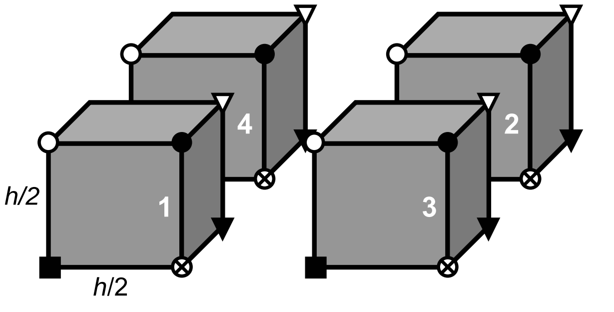

■ $\dot{U}$, ρ_U^A

▼ $\dot{V}$, ρ_V^A

● $\dot{W}$, ρ_W^A

□ $T_{xy} = T_{yx}$, μ_{xy}^H, ξ_l^{xy}, $Y_l^{\mu xy}$

▽ $T_{yz} = T_{zy}$, μ_{yz}^H, ξ_l^{yz}, $Y_l^{\mu yz}$

○ $T_{zx} = T_{xz}$, μ_{zx}^H, ξ_l^{zx}, $Y_l^{\mu zx}$

⊗ T_{xx}, T_{yy}, T_{zz}, μ^H, κ^H, ξ_l^{xx}, ξ_l^{yy}, ξ_l^{zz}, Y_l^{μ}, Y_l^{κ}

$l = 1, \ldots, 4$

Figure 1. Spatial distribution of the material parameters and field functions.

correspond to the ratio of the shear-wave velocities in the stiffer bedrock and softer sediments. Therefore we developed and algorithm that enables to adjust a discontinuous spatial grid accordingly except that, due to the structure of the staggered grid, the ratio of the spatial grid spacings in the coarser and finer grids has to be an odd number. In other words, depending on the model of medium, we can choose a 1:1 (uniform) grid, or 1:3, 1:5, ... discontinuous grid. The grid is illustrated in Fig. 2.

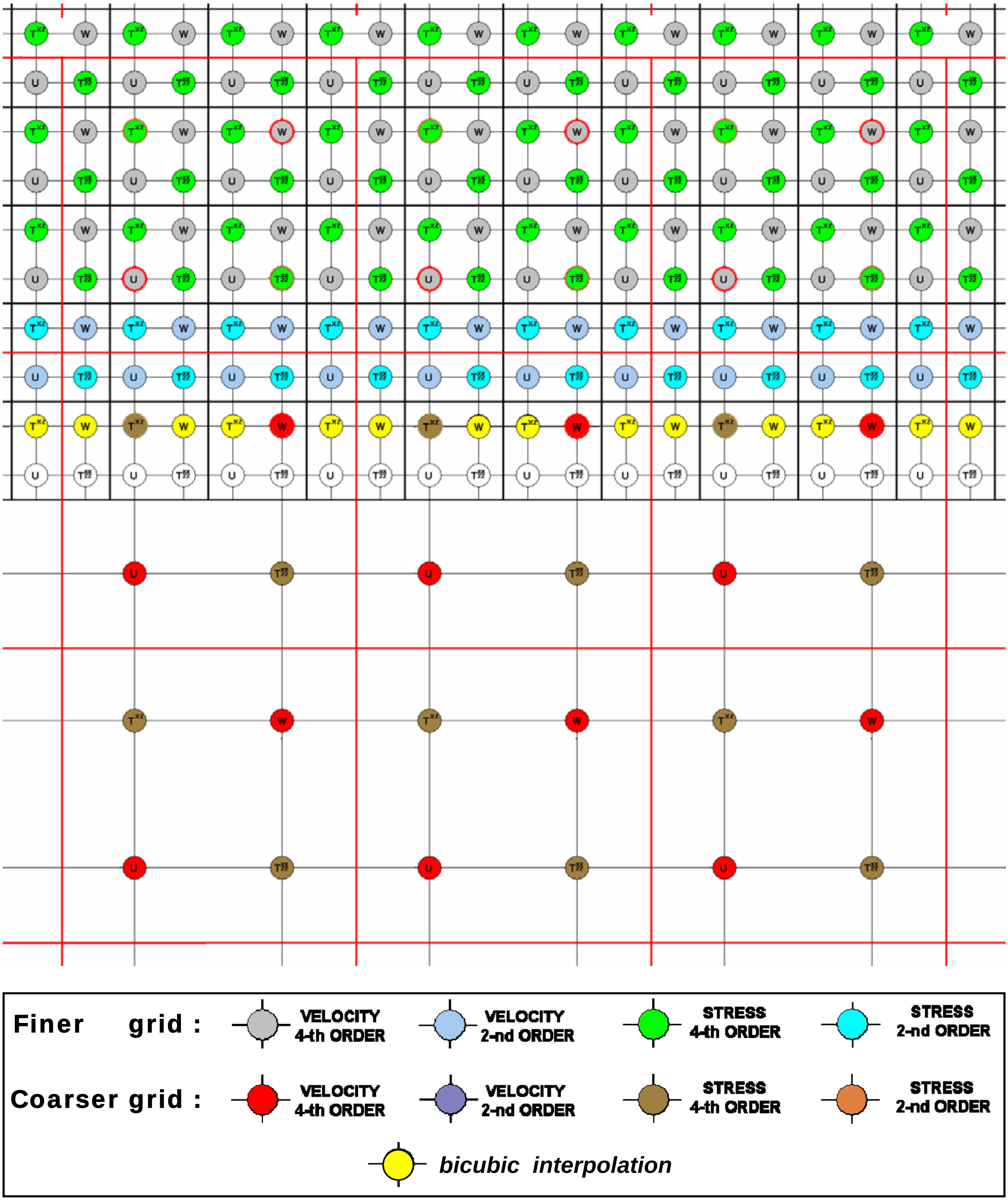

Figure 2. Arbitrary discontinuous staggered grid (case 1 : 3).

4. Computer Code

A Fortran 95 computer code 3DFD_VS has been developed for performing the finite-difference scheme. A PML absorbing boundary conditions are implemented. The code is MPI parallelized. The code is available at http://www.nuquake.eu/Computer_Codes/ .

5. Model of Medium

Model of the medium used for simulations of seismic motion is that constructed by Vallon (1999) with flat free surface. A bedrock depth was obtained by inverting gravimetric measurements. Geometry of the sediment-bedrock interface and material parameters are shown in Fig. 3.

6. Configuration of Sources and Receivers

Four different sources were prescribed in the benchmark. Source W1 represents weak right-lateral strike-slip event (Mw=2.9) on the Eastern Part of the Belledonne Border Fault, source W2 left-lateral strike-slip event (Mw=2.8) on the Southern Part of the Belledonne

Geometry of the Sediment-bedrock Interface

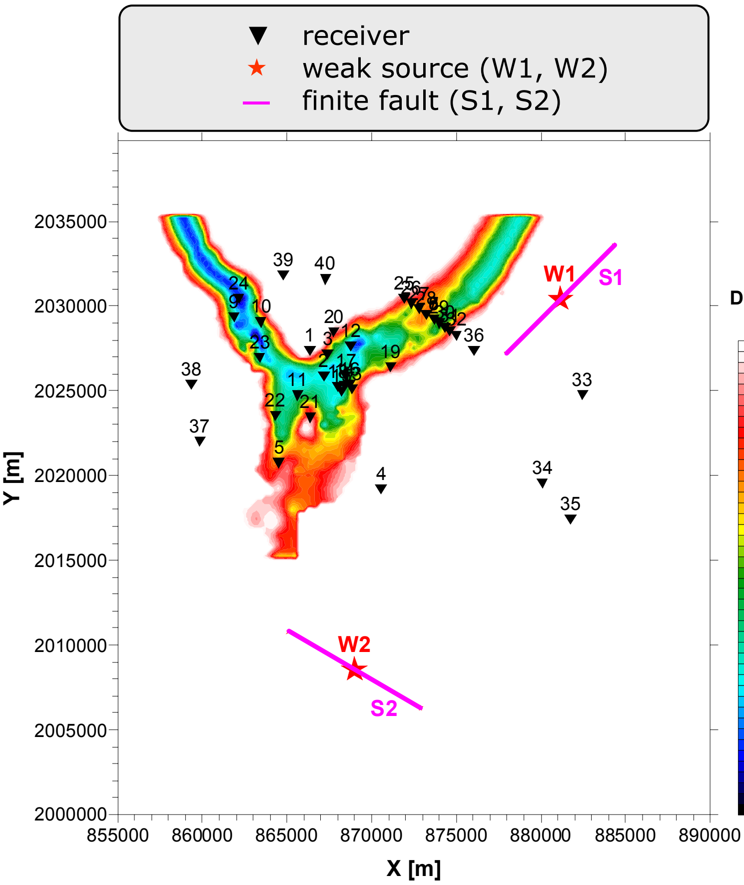

Material Parameters

Depth of top of a layer [m]	VP [m/s]	VS [m/s]	Density [kg/m^3]	Quality factor
0	5 600	3 200	2 720	∞
3 000	5 920	3 430	2 720	∞
27 000	6 600	3 810	2 920	∞
35 000	8 000	4 450	3 320	∞

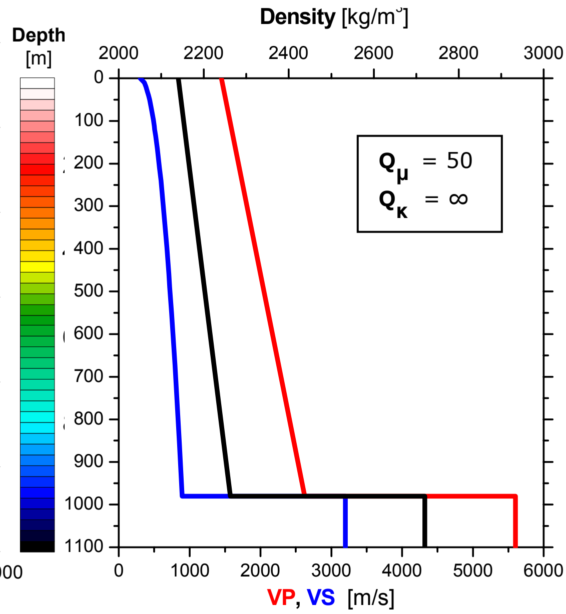

Figure 3. Model of the medium and positions of sources and receivers.

Border Fault. Sources S1 and S2 are the strong alternatives of W1 and W2 (Mw=6.0) with Haskel crack on the fault with dimensions 4.5 km x 9 km. Benchmark participants were requested to provide time series of ground velocity at 40 receivers (Fig. 3).

7. Simulation and Results

All simulations where performed on small cluster of Opteron2.2 machines (6 CPUs, 10GB RAM in total). A discontinuous grid with finer grid of 1321x1431x45 grid cells and 25 m grid spacing, and coarser grid of 265x287x65 grid cells and 125 m grid spacing were used. As a consequence, the maximum frequency is around 2.5 Hz. The computational time for 30s time window (weak cases W1 and W2) was 33 hours, for 80s time window (strong cases S1 and S2) 88 hours. The peak-ground-velocity maps and velocity seismograms (vertical component) at the receivers #25 to #32 on the 2D profile are displayed in the Figs. 4 – 7.

8. Acknowledgement

This work was supported by the EU Marie Curie research program SPICE (Seismic Wave Propagation and Imaging in Complex media: a European Network)

9. References

Bielak, J., Loukakis, K., Hisada, Y., Yoshimura, Ch. 2003. Domain reduction method for three-dimensional earthquake modeling in localized regions. Part I: Theory. Bull. Seism. Soc. Am., 93 (2), 817-824.

Chaljub, E., Komatitsch, D., Vilotte, J. P., Capdeville, Y., and Festa, G., 2006. Spectral Element Analysis in Seismology. In Advances in Wave Propagation in Heterogeneous Earth, R.-S. Wu,V. Maupin, R. Dmowska, eds., in the series 'Advances in Geophysics, Vol. 48', Elsevier – Pergamon.

Kang, T.-S. and Ch.-E. Baag, 2004b. An efficient finite-difference method for simulating 3D seismic response of localized basin structures. Bull. Seism. Soc. Am., 94, 1690-1705.

Käser, M., Dumbser, M., 2006. An arbitrary high-order discontinuous Galerkin method for elastic waves on unstructured meshes - I. The two-dimensional isotropic case with external source terms. Geophys. J. Int. 166 (2), 855-877.

Komatitsch, D., Liu, Q., Tromp, J., Suss, P., Stidham, C., Shaw, J. H., 2004. Simulations of ground motion in the Los Angeles basin based upon the spectral element method. Bull. Seism. Soc. Am., 94, 187-206.

Kristek, J., Moczo, P., 2003. Seismic wave propagation in viscoelastic media with material discontinuities – a 3D 4th-order staggered-grid finite-difference modeling. Bull. Seism. Soc. Am., 93(5), 2273-2280.

Kristek, J., Moczo, P., Archuleta, R. J., 2002. Efficient methods to simulate planar free surface in the 3D 4th-order staggered-grid finite-difference schemes. Studia Geophys. Geod., 46, 355-381.

Moczo, P., Kristek, J., Vavryčuk, V., Archuleta, R. J., Halada, L., 2002. 3D heterogeneous staggered-grid finite-difference modeling of seismic motion with volume harmonic and arithmetic averaging of elastic moduli and densities. Bull. Seism. Soc. Am., 92(8), 3042-3066.

Moczo, P., Kristek, J., Gális, M., 2004. Simulation of planar free surface with near-surface lateral discontinuities in the finite-difference modeling of seismic motion. Bull. Seism. Soc. Am. 94(2), 760-768.

Moczo, P., Kristek, J., 2005. On the rheological models used for time-domain methods of seismic wave propagation. Geophys. Res. Lett. 32, L01306, doi: 10.1029/2004GL021598.

Takeuchi, N. and R. J. Geller, 2000. Optimally accurate second order time-domain finite difference scheme for computing synthetic seismograms in 2-D and 3-D media. Phys. Earth Planet. Int. 119, 99-131.

Yoshimura, Ch., Bielak, J., Hisada, Y., Fernández, A., 2003. Domain reduction method for three-dimensional earthquake modeling in localized regions. Part II: Verification and applications. Bull. Seism. Soc. Am., 93 (2), 825-840.

Vallon, M., 1999.Estimation de l'épaisseur d'alluvions et sédiments quaternaires dans la région grenobloise par inversion des anomalies gravimétriques. LGGE, Université Joseph Fourier, pp. 33.

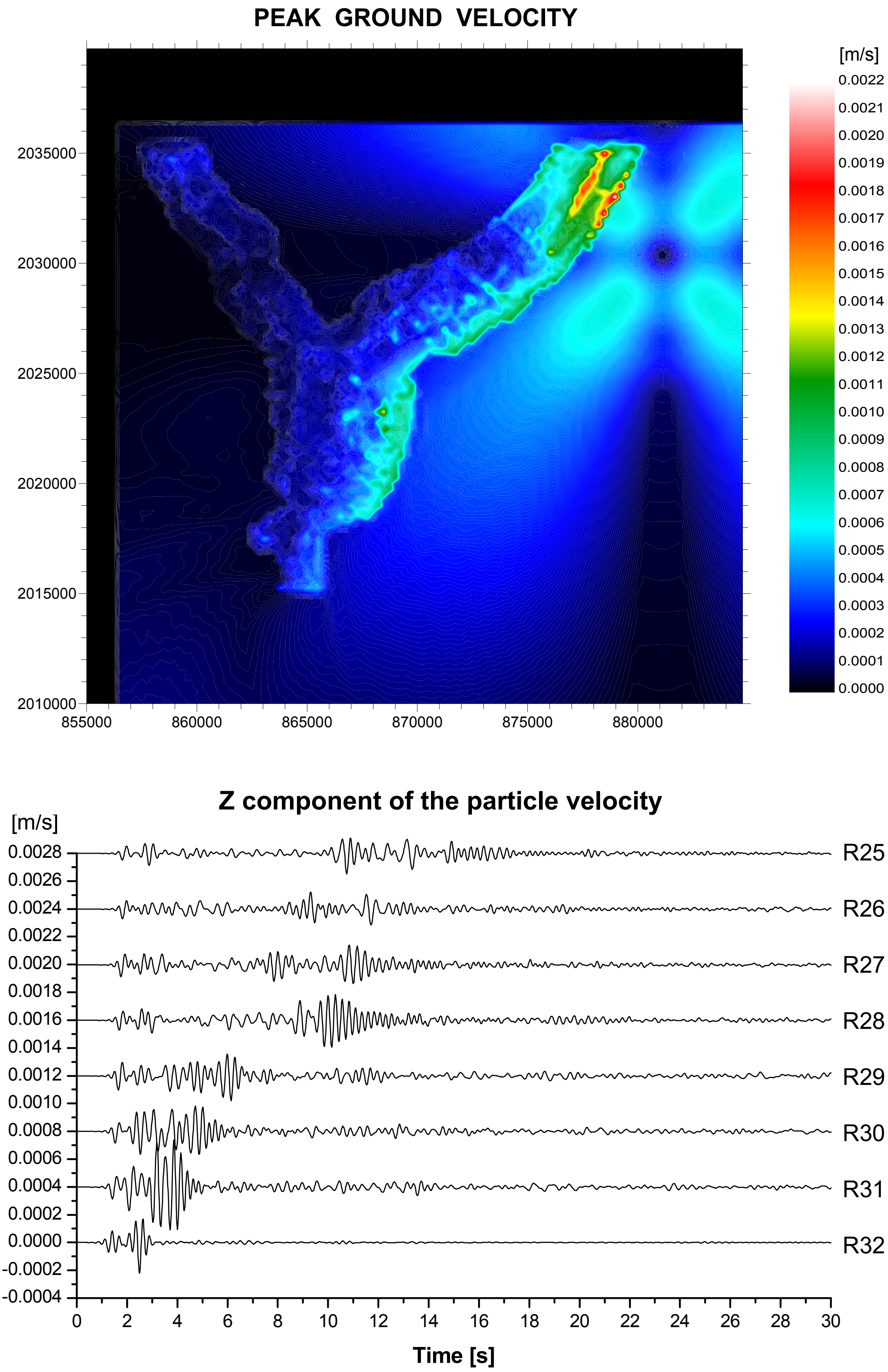

*Figure 4. Simulation **W1:** (top) The peak-ground-velocity map,*
(bottom) velocity seismograms of the vertical component of the particle velocity.

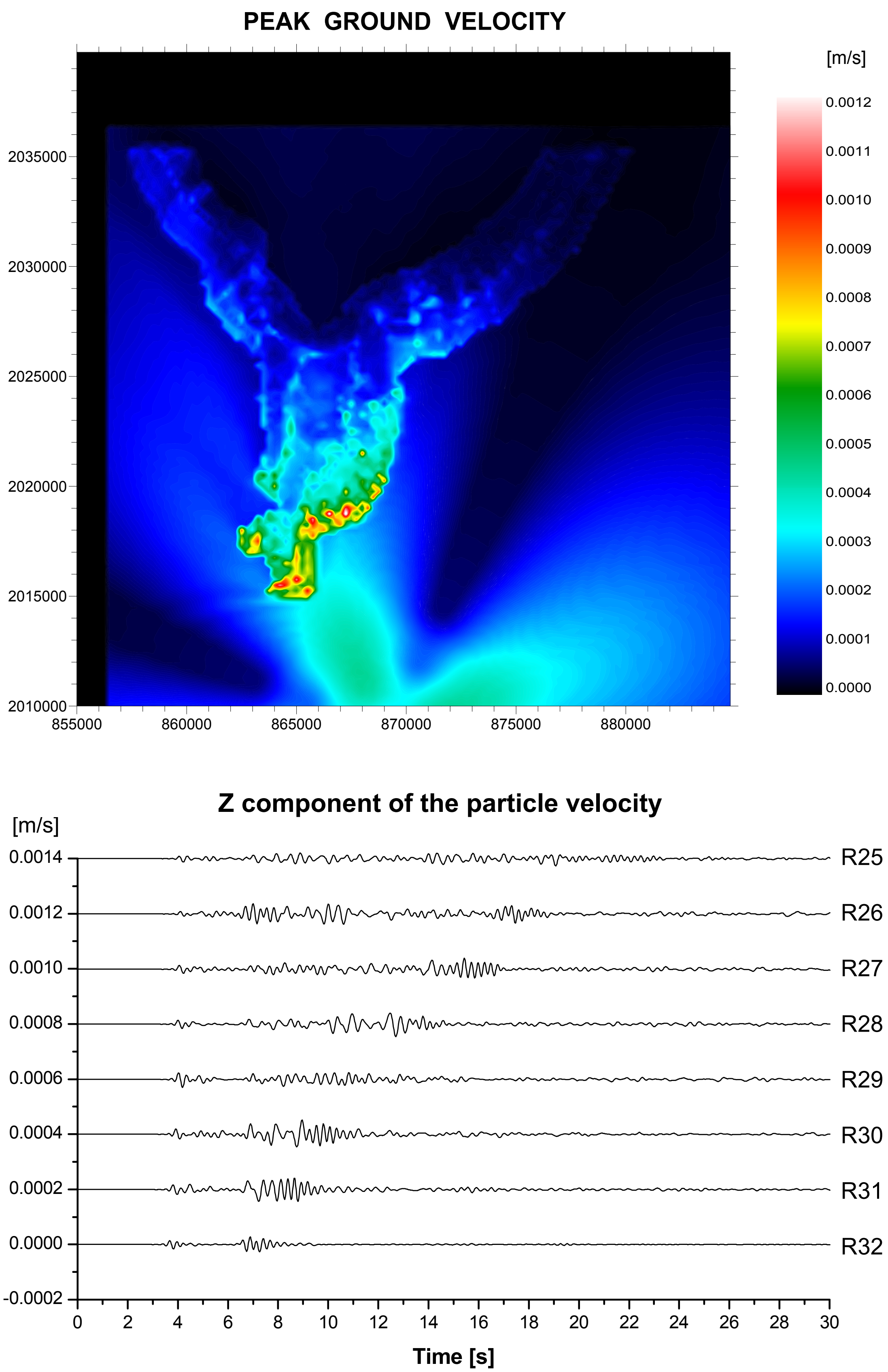

*Figure 5. Simulation **W2:** (top) The peak-ground-velocity map, (bottom) velocity seismograms of the vertical component of the particle velocity.*

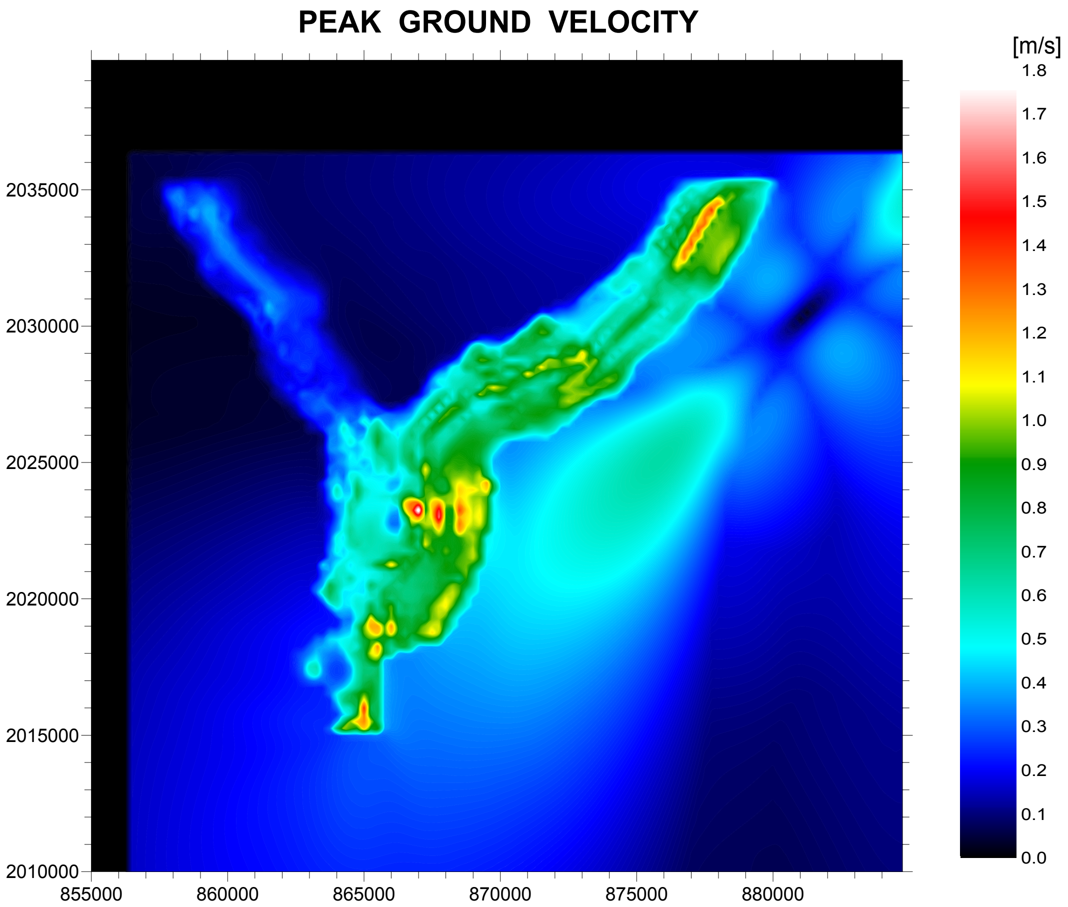

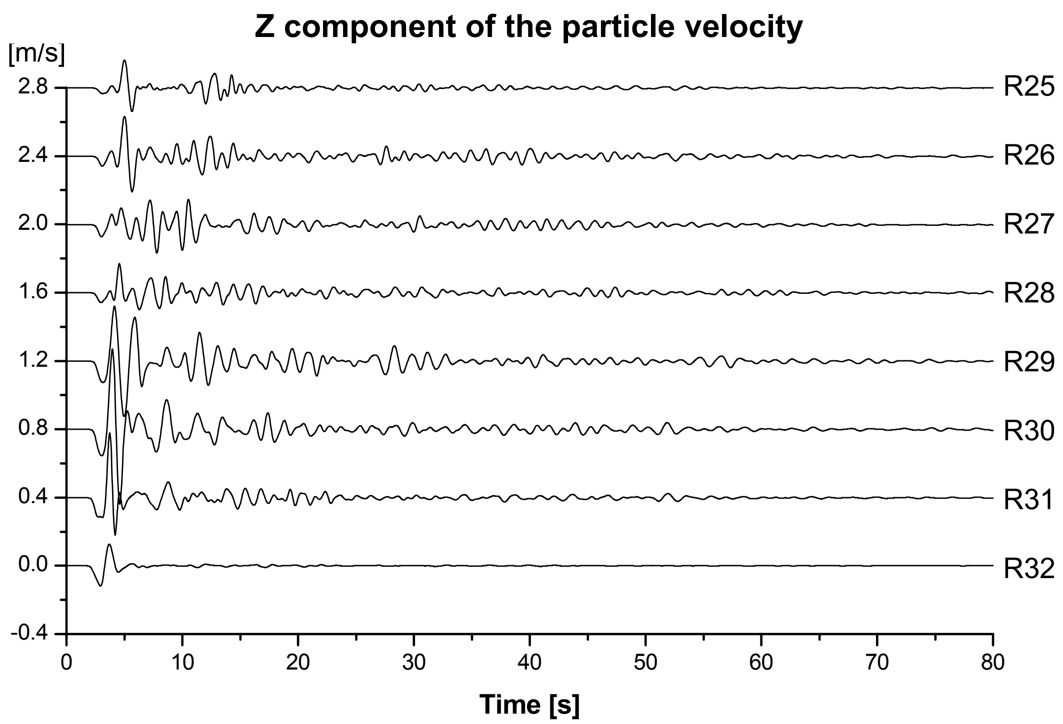

*Figure 6. Simulation **S1:** (top) The peak-ground-velocity map, (bottom) velocity seismograms of the vertical component of the particle velocity.*

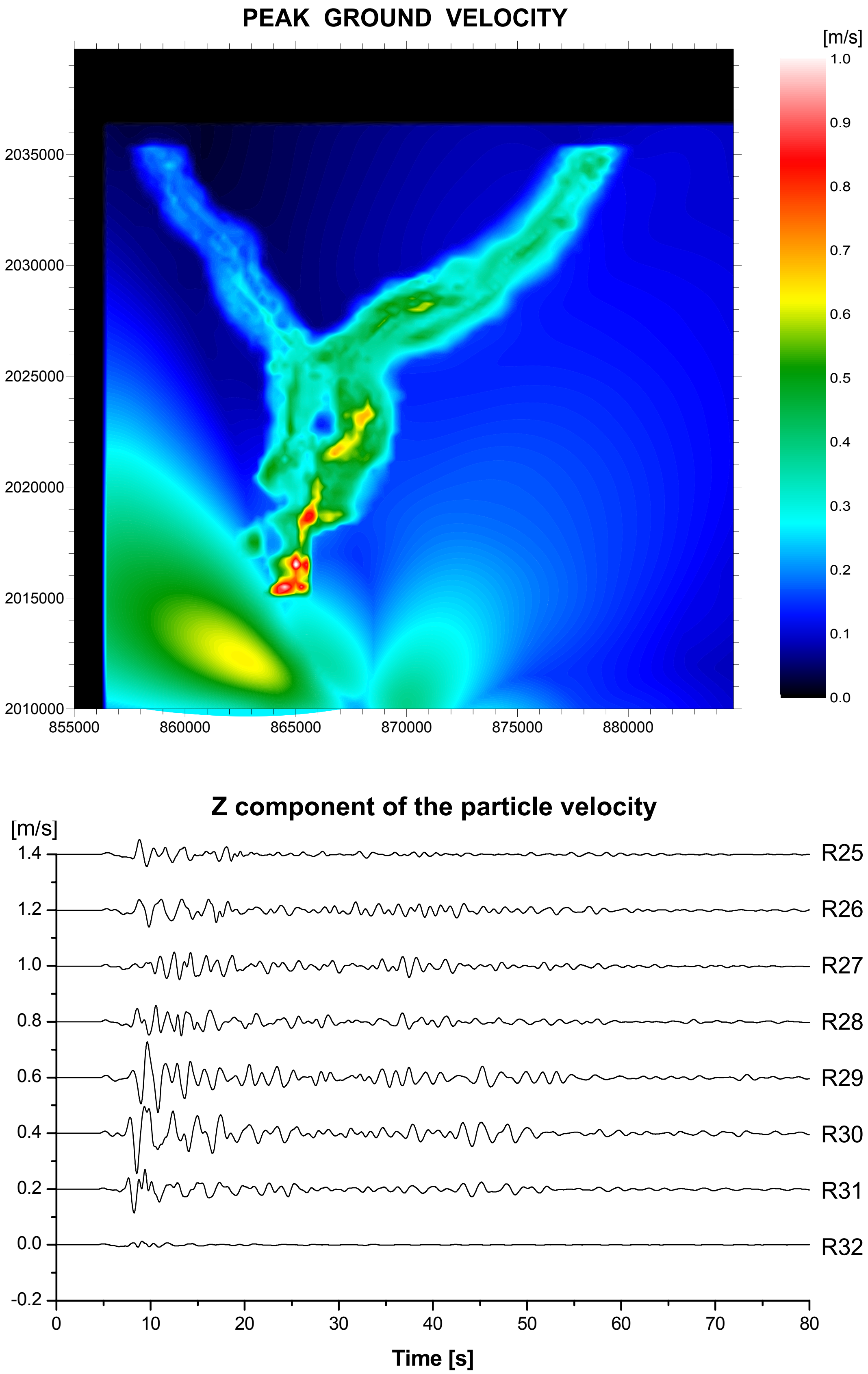

Figure 7. Simulation ***S2:*** *(top) The peak-ground-velocity map, (bottom) velocity seismograms of the vertical component of the particle velocity.*